

# Elliptic flow from colour strings

M.A.Braun<sup>a,b</sup>, C.Pajares<sup>a</sup>

<sup>a</sup> University of Santiago de Compostela, Spain,

<sup>b</sup> S.Petersburg State University, Russia

December 5, 2018

**Abstract** It is shown that the elliptic flow can be successfully described in the colour string picture with fusion and percolation provided anisotropy of particle emission from the fused string is taken into account. Two possible sources of this anisotropy are considered, propagation of the string in the transverse plane and quenching of produced particles in the strong colour field of the string. Calculations show that the second source gives an overwhelming contribution to the flow at accessible energies.

## 1 Introduction

The observed elliptic flow in heavy-ion collisions can be conveniently understood if the distribution of the observed particles depends not only on the physical conditions realized locally at their production point but also on the global geometry of the event. In a relativistic local theory this non-local information can only emerge as a collective effect, requiring interaction between the relevant degrees of freedom localized at different points in the collision region. In this sense anisotropic flow is a particularly unambiguous and strong manifestation of collective dynamics in heavy-ion collisions. The large elliptic flow coefficient  $v_2$  can be qualitatively understood as follows. In a high-energy collision spectator nucleons are fast enough to move away leaving behind at mid-rapidity an almond shaped azimuthally asymmetric overlap region filled with the QCD matter. This spatial asymmetry implies unequal pressure gradients in the transverse plane, with a larger density gradient perpendicular to the reaction plane (in-plane). As a consequence of the subsequent multiple interactions between the degrees of freedom involved, the spatial asymmetry leads to anisotropy in the momentum space [1]. The final particle transverse momenta are more likely to lie in the in-plane than in the perpendicular direction, which leads to  $v_2 > 0$  as predicted in [2].

This general idea has been realized in various mechanisms for the source of elliptic flow. A convenient and successful way to describe the flow anisotropy is achieved in the hydrodynamical approach, taking into account the unsymmetric shape of the nuclei overlap in the transverse plane at values of the impact parameter  $\mathbf{b}$  different from zero. This description of course assumes collective effects to be responsible for the flow. The flow can also be explained in different terms as following from the quenching of initially produced particles in the nuclear matter. Since the path inside the nuclear overlap of particles emitted along  $\mathbf{b}$  and orthogonal to it is different, the observed dependence on the azimuthal angle  $\phi$  of emission is natural. Finally in [3] the authors pointed out that the origin of the flow may be already contained in the asymmetry of the initial emission, before any collective effects have taken place. They used the Regge picture of particle production and showed that the flow may follow from the dependence of the effective emission vertex on the

angle between the directions of the emitted particle momentum  $\mathbf{p}$  and pomeron propagation  $\mathbf{e}$ . In the end the strength of the flow, characterized by the standard coefficient  $v_2$  was related to the model dependent coefficient  $\epsilon$  in the dependence on  $(\mathbf{pe})^2$ .

In this note we want to draw attention that the elliptic flow can also be naturally explained in the colour string approach, duly generalized to include string fusion and percolation [4, 5, 6, 7]. This approach has proved to be quite successful in the description of particle production and correlations in the soft part of spectra [8, 9, 10]. In the original formulation in which strings were assumed to be just points in the transverse space there was no place for elliptic flow whatever the string distribution in the nuclei overlap. However such a picture is of course too simplified. It neglects at least two circumstances. First, strings can propagate in the transverse space and so be characterized by a vector in this space rather than a point. In the Regge language this corresponds to assuming that the pomeron slope  $\alpha'$  is substantially different from zero, in contrast to the original assumption that the slope is quite small. In the 3-dimensional space the string becomes not orthogonal to the transverse plane and one may expect an anisotropic emission of particles in this plane and a non-zero elliptic flow. This mechanism is quite similar to the one considered in [3] with the anisotropy created already in the initial emission. Of course the actual form of this anisotropy cannot be established on purely theoretical grounds but has to be taken in a semiphenomenological manner. We study possible forms of this anisotropy and compare it with the experimental situation. Our conclusion is that with any choice of anisotropy in the emission of the string the final elliptic flow is far too small as compared to the experimental data. So our conclusion is that taking into account only the flow from the initial emission, one cannot explain the data. Inclusion of collective effects in the form of consecutive interactions seems to be unavoidable.

This motivated us to study an alternative mechanism of azimuthal anisotropy, using the second circumstance characteristic for a realistic string picture, namely that the string is not point-like in the transverse plane but occupies a certain non-zero area in the transverse space and that a fused string occupies a greater area than the simple string. Then partons emitted at some point inside the string have to pass a certain length before they appear outside and are observed. It is natural to assume that as they pass through the strong colour field inside the string they emit gluons and their energy diminishes. As a result, the particle observed with transverse momentum  $p$  outside the string has to be born with a greater momentum inside the string, whose value depends on the path length travelled inside the string and so different for different direction of emission. In its spirit, this mechanism is similar to that of particle quenching in the nuclear matter giving the string explanation and characteristics of this quenching. Our calculations confirm that a sizable elliptic flow follows from this mechanism. Its centrality and transverse momentum dependence agrees with the behaviour of the RHIC data [13, 14, 15, 16]. These results also confirm the ones obtained in a similar framework using different simplified methods [17, 18]

## 2 A string stretched between points $\beta_1$ and $\beta_2$

We consider a model in which strings can be formed between different points in the transverse plane, say,  $\beta_1$  in the projectile nucleus and  $\beta_2$  in the target one. Here  $\beta_{1,2}$  are in fact two-dimensional vectors, which we do not specifically mark in the following. The probability to form such a string will be given by the distribution in  $\beta = \beta_1 - \beta_2$  of the soft pomeron

$$P(y, \beta) = \frac{1}{4\pi\alpha'y} e^{\epsilon y - \beta^2/(4\alpha'y)}. \quad (1)$$

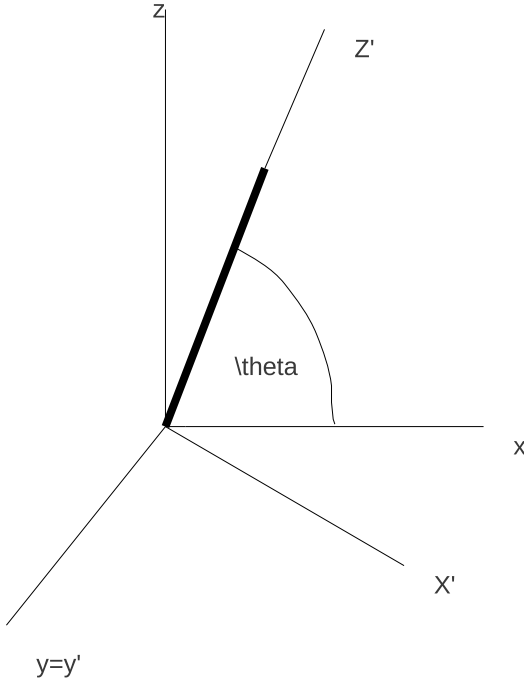


Figure 1: The string in the 3-dimensional space. The shown angle is  $\theta = \pi/2 - \theta'$

Obviously the pomeron extends to larger distances as  $y$  grows, the average distance being  $\langle \beta \rangle = \sqrt{4\alpha'y}$ . This will be also the average length of the string in the transverse plane.

We shall be interested in the distribution of particles emitted from such a string. To see it we have to recall that the string has also some dimension along the  $z$ -axis. We assume that the string is located in the  $xz$ -plane and its direction defines the  $z'$  axis in the primed coordinate system  $(x', y', z')$ . The  $y'$  axis is assumed to coincide with the  $y$  axis in the original system and the  $x'$  axis is taken to be orthogonal to  $y'$  and  $z'$  axes (see Fig.1).

Our initial assumption, borrowed from the Schwinger mechanism of particle emission in the external field, is that particles are emitted isotropically only in the plane orthogonal to the string direction. So in the primed system we find that the probability to emit a particle with momentum  $p'$  is

$$\mu'(y, p') = \delta(p'_z) \frac{\xi}{\pi} e^{-\xi(p'^2_x + p'^2_y)}. \quad (2)$$

To find the distribution in the original system we have to express  $p'$  via the momentum  $p$  in the original system, that is to make a rotation by angle  $\theta'$  between the two systems. We find the distribution of emitted particles in  $p_\perp$  in the original system as

$$\mu(y, p_\perp) = \frac{\xi}{\pi \cos \theta'} e^{-\xi(p_y^2 + p_x^2 / \cos^2 \theta')}. \quad (3)$$

Angle  $\theta'$  is given by

$$\theta' = \arctan \frac{\beta}{\Delta z}. \quad (4)$$

As we have seen, on the average  $\beta \sim \sqrt{\alpha' y}$  and grows with energy of the string  $W = e^{y/2}$ . The length in  $z$  can be estimated as  $1/W = e^{-y/2}$ . So angle  $\theta'$  is quite close to  $\pi/2$ . Putting  $\theta' = \frac{\pi}{2} - \theta$  we find that  $\theta$  is small and diminishes with energy:

$$\theta \simeq \frac{\Delta z}{\beta} \sim \frac{e^{-y/2}}{\sqrt{\alpha' y}}. \quad (5)$$

This means that unless  $\alpha' = 0$  the string only radiates in the direction of  $y$ , so that

$$\mu(y, p_\perp) = \sqrt{\frac{\xi}{\pi}} \delta(p_x) e^{-\xi p_y^2} = \sqrt{\frac{\xi}{\pi}} \delta(p_x) e^{-\xi(p_\perp^2 - \frac{(p_\perp \beta)^2}{\beta^2})}. \quad (6)$$

On the other hand, if  $\alpha' = 0$  then  $\theta' = 0$ ,  $\theta = \pi/2$  and we return to the old case of string characterized by a single impact parameter with the emission probability

$$\mu(y, p_\perp)_{\alpha'=0} = \frac{\xi}{\pi} e^{-\xi p_\perp^2}. \quad (7)$$

Obviously with  $\alpha' \neq 0$  emission is anisotropic and we expect a non-zero elliptic flow effect.

One has to understand that this ideal case may have little to do with the realistic behaviour of the string, which does not exactly conform to the Schwinger mechanism, since its dimensions are finite. To come somehow closer to reality we may soften our assumption that the string does not emit particles along its axis at all. Instead we may assume that emission along the axis is simply different from emission in the transverse plane, so that the three-dimensional distribution in the primed system is

$$\mu(y, p') = \sqrt{\eta} \left(\frac{\xi}{\pi}\right)^{3/2} e^{-\xi(\eta p_x'^2 + p_y'^2 + p_z'^2)}, \quad (8)$$

where  $\eta$  shows the difference in emission along the string and orthogonal to it. If  $\eta > 1$  the emission along the string is damped. In the limit  $\eta \rightarrow \infty$  we return to the previous case of an ideal string. If  $\eta < 1$  then, on the contrary, emission along the string direction is enhanced. The same distribution in the original system is easily obtained expressing the primed momenta via the ones in the original system. The final distribution in the transverse momentum  $p_\perp$  is obtained after integration over  $p_z$  and we find

$$\mu(y, p_\perp) = \int dp_z \mu(y, p) = \frac{\xi \sqrt{\gamma}}{\pi} \exp\left(-\xi(p_y^2 + \gamma p_x^2)\right), \quad (9)$$

where the final excentricity parameter  $\gamma$  is

$$\gamma = \frac{\xi}{\cos^2 \theta + \xi \sin^2 \theta} \quad (10)$$

and we used  $\theta' = \pi/2 - \theta$

In the high-energy limit when  $\theta \rightarrow 0$  we now find  $\gamma = \eta$  and

$$\mu(y, p_\perp) = \frac{\xi}{\pi} \sqrt{\eta} \exp \left[ -\xi \left( p_y^2 + \eta p_x^2 \right) \right]. \quad (11)$$

If  $\alpha' = 0$  we have  $\theta = \pi/2$ ,  $\gamma = 1$  and

$$\mu(y, p_\perp) = \frac{\xi}{\pi} \exp \left[ -\xi \left( p_y^2 + p_x^2 \right) \right]. \quad (12)$$

Obviously with  $\gamma$  different from unity the anisotropy is fully determined by its value.

### 3 Elliptic flow from independent strings

Once emission from a string is anisotropic, it is obvious that we shall find a non-zero elliptic flow in AB scattering. The derivation closely follows [3]. Let the probability to find a string attached to point  $\beta_1$  in the projectile nucleus A to be

$$P_A(\beta_1) = \int d^2 b_1 T_A(b_1) t(\beta_1 - b_1), \quad (13)$$

where  $T_A$  is the profile function, and a similar probability  $P_B(\beta_2)$  to find a string attached to point  $\beta_2$  in the target nucleus

$$P_B(\beta_2) = \int d^2 b_2 T_B(b_2) t(\beta_2 - b_2), \quad (14)$$

where  $b$  is the impact parameter of the collision. The probability to find a string stretched between the points  $\beta_1$  and  $\beta_2$  will be determined by the factor  $p(\beta_1 - \beta_2)$ , where

$$p(\beta) = \frac{1}{4\pi\alpha'y} \exp \left( -\frac{\beta^2}{4\alpha'y} \right). \quad (15)$$

So the final distribution of emitted particles will be

$$M(b, p) = \int d^2 \beta_1 d^2 \beta_2 P_A(\beta_1) P_B(\beta_2) p(\beta_1 - \beta_2) \mu(y, \beta, p_\perp), \quad (16)$$

where  $\mu$  is given by (9) with the  $x$ -axis along the direction of the string, that is, along  $\beta = \beta_1 - \beta_2$

One can transform (16) to the form introduced in [3]:

$$M(b, p) = \int d^2 \beta T_{int}(b - \beta) \Gamma(\beta, y, p_\perp), \quad (17)$$

where obviously

$$T_{int}(b) = \int d^2 \beta_1 P_A(\beta_1) P_B(\beta - \beta_1) \quad (18)$$

and

$$\Gamma(\beta, y, p_\perp) = p(\beta) \mu(\beta, y, p_\perp), \quad (19)$$

with

$$\mu(\beta, y, p_\perp) = \frac{\xi \sqrt{\gamma}}{\pi} \exp \left[ -\xi \left( p^2 - \frac{(p\beta)^2}{\beta^2} + \gamma \frac{(p\beta)^2}{\beta^2} \right) \right]. \quad (20)$$

Taking the final  $x$ -axis along the direction of  $p_\perp$  we get the expression which can be compared with [3]

$$\Gamma(\beta, p_\perp) = \frac{\xi\sqrt{\gamma}}{4\pi^2\alpha'y} \exp \left[ -\frac{\beta^2}{4\alpha'y} - \xi p^2 (\sin^2 \chi + \gamma \cos^2 \chi) \right], \quad (21)$$

where  $\chi$  is the azimuthal angle between  $\beta$  and  $p_\perp$ .

As compared to [3] the role of  $p^2$  and  $\beta^2$  are reversed in our approach. In our case the distribution  $\Gamma$  is essentially

$$\Gamma \sim e^{-\beta^2/\beta_0^2 - \xi p^2 (\sin^2 \chi + \gamma \cos^2 \chi)}, \quad (22)$$

where  $\beta_0^2 = 4\alpha'y$  and excentricity  $\gamma$  is given by Eq. (10) (it depends (weakly) on the string dimension  $\beta$ ). In [3] one has

$$\Gamma \sim e^{-\xi p^2 - (\beta^2/\beta_0)(\sin^2 \chi + \gamma \cos^2 \chi)}, \quad (23)$$

where  $\beta_0$  and  $\gamma$  are expressed via parameters of the emission vertex in the Regge approach

$$\beta_0 = 2r_q, \quad \gamma = \frac{r_q^2}{r_q^2 + \epsilon r_0^4 p^2}, \quad (24)$$

with  $r_q \sim r_0 \sim 1$  fm. In [3]  $\gamma$  depends on  $p^2$  (not weakly).

However it turns out that after integration over  $\phi$  both forms are essentially equivalent. The main difference in the results comes from the choice of parameters. In particular with the standard choice of the pomeron slope  $\alpha' = 0.2$  GeV<sup>-2</sup> our  $\beta_0$  turns out to be quite small at accessible rapidities as compared to the value assumed in [3] and becomes of the same magnitude only at  $y \sim 100$

## 4 Strings homogeneously distributed

### 4.1 Analytic expressions

To obtain concrete results we have to specify the distributions of strings inside the nuclei. For simplicity we assume strings to be homogeneously distributed in the transverse plane inside the nucleus:

$$P_A(\beta_1) = N_s \frac{\theta(R_A - \beta_1)}{\pi R_A^2}, \quad (25)$$

where  $N_s$  is the number of strings and  $R_A$  is the nucleus radius. We also consider a simple case of a collision of two identical nuclei, so that, up to coefficient,  $T_{int}$  is just the overlap area of the nuclei at distance  $\beta$  between their centers:

$$T_{int}(\beta) = \frac{N_s^2}{\pi^2 R_A^2} (2\zeta - \sin(2\zeta)), \quad \zeta = \arccos \frac{\beta}{2R_A}. \quad (26)$$

For the distribution in angle  $\phi$  between  $p$  and  $b$  the coefficients in front of the inclusive cross-section are unimportant. So for our purpose we find

$$M(b, p) = \int_0^{\beta_m} \int_0^{2\pi} d\chi (2\zeta - \sin(2\zeta)) e^{-\beta^2/\beta_0^2} e^{-\xi p^2 (\sin^2 \chi + \gamma \cos^2 \chi)}, \quad (27)$$

where

$$\beta_m = 2R_A + b, \quad \beta_0 = 4\alpha'y, \quad \zeta = \arccos \frac{|b - \beta|}{2R_A}, \quad (28)$$

$\gamma$  is given by Eq. (10). and  $\xi$  is the inverse string tension which determines the distribution in momenta. The dependence of  $M(b, p)$  on  $\phi$  comes from function  $\zeta$ . If we put  $\chi = \chi' + \phi$  then

$$\zeta = \arccos \frac{\sqrt{b^2 + \beta^2 - 2b\beta \cos \chi'}}{2R_A} \quad (29)$$

and we get

$$M(b, p) = \int_0^{\beta_m} \int_{-\pi}^{\pi} d\chi' \left( 2\zeta - \sin(2\zeta) \right) e^{-\beta^2/\beta_0^2} e^{-ap^2(\sin^2(\chi'+\phi) + \gamma \cos^2(\chi'+\phi))}, \quad (30)$$

where integration over  $\chi'$  should be restricted by the condition

$$|\chi'| < \arccos \frac{b^2 + \beta^2 - 4R_A^2}{2b\beta} \quad (31)$$

unless the argument of the arccos is less than  $-1$ .

## 4.2 Numerical results

We take the standard value for  $\alpha' = 0.2 \text{ GeV}^{-2}$ . For the string tension  $\xi$  we choose  $\xi = 0.25 \text{ GeV}^{-2}$ . The only left parameter is excentricity  $\gamma$ . From the start one finds that with values of  $\gamma$  greater than unity we obtain negative values for the elliptic flow parameter  $v_2$  and with values of  $\gamma$  less than unity we get positive values of  $v_2$ . Should the elliptic flow come only from the discussed effect of string extension in the transverse plane, the experimental data would exclude  $\gamma > 1$  and thus the naive picture in which the string only emits particles in the plane transverse to its direction, as in the Schwinger picture. Rather we have to admit the opposite: the string emits particles predominantly along its direction, which leads to  $\gamma < 1$ . This does not look too exotic if the length of the string in the  $z$ -direction is much smaller than in its transverse direction.

However both with  $\gamma < 1$  and  $\gamma > 1$  the magnitude of the elliptic flow turns out to be quite small at accessible rapidities. We studied Au-Au collisiona at rapidity  $y = 10$ . In Fig. 2 and 3 we show our results with  $\gamma = 0.1$  which lead to positive values for  $v_2$ . In Fig. 2 we show  $v_2$  as a function of impact parameter  $b$  at different values of  $p$ . In Fig.3 we illustrate the  $p$  dependence of the elliptic flow at  $b = 6$ . As we see the qualitative behaviour of both  $b$ - and  $p$ - dependence of the elliptic flow agrees with the experimental findings. However values of  $v_2$  at not too peripheral collisions are ten to twenty times lower than the data. Only in the limiting case of a very small overlap these values become comparable to the observed ones.

In (4) we show the elliptic flow for  $\gamma = 10$ , when the resulting  $v_2$  is negative. Its values turn out to be practically independent of  $p$ . The magnitude of  $|v_2|$  and its behaviour with  $b$  are very similar to what we have obtained for values of  $\gamma$  smaller than unity. Again  $|v_2|$  reaches value of the order of several percents only at very peripheral collisions.

## 5 String fusion as a source of elliptic flow

### 5.1 The model

As we have seen, propagation of strings in the transverse plane gives a certain contribution to the elliptic flow, but it is too small compared to the experimental data and can only be noticeable at extremely peripheral collisions. So we pass to another source of elliptic flow related to the process

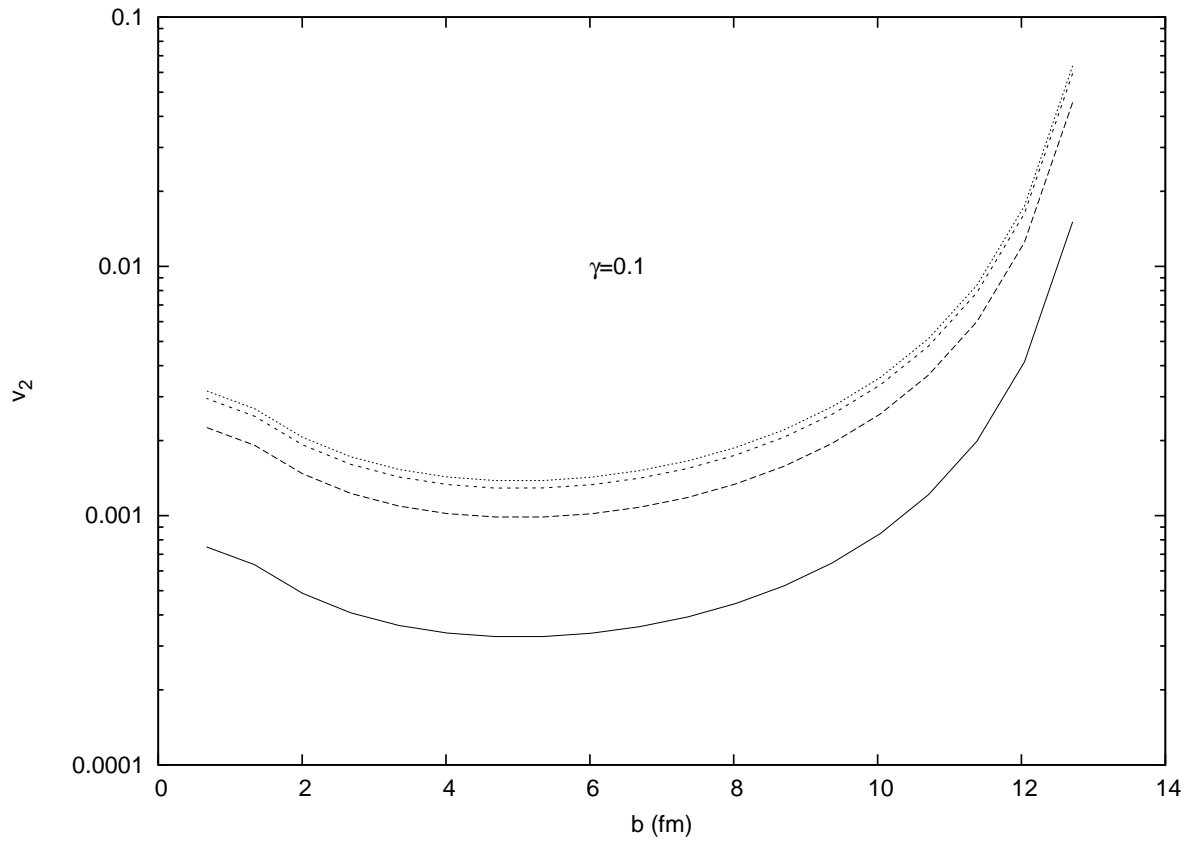


Figure 2: Elliptic flow coefficient  $v_2$  with  $\gamma = 0.1$  as a function of  $b$  for Au-Au collisions at  $y = 10$ . The curves from bottom to top correspond to  $p = 0.5, 1.15$  and  $2$  GeV



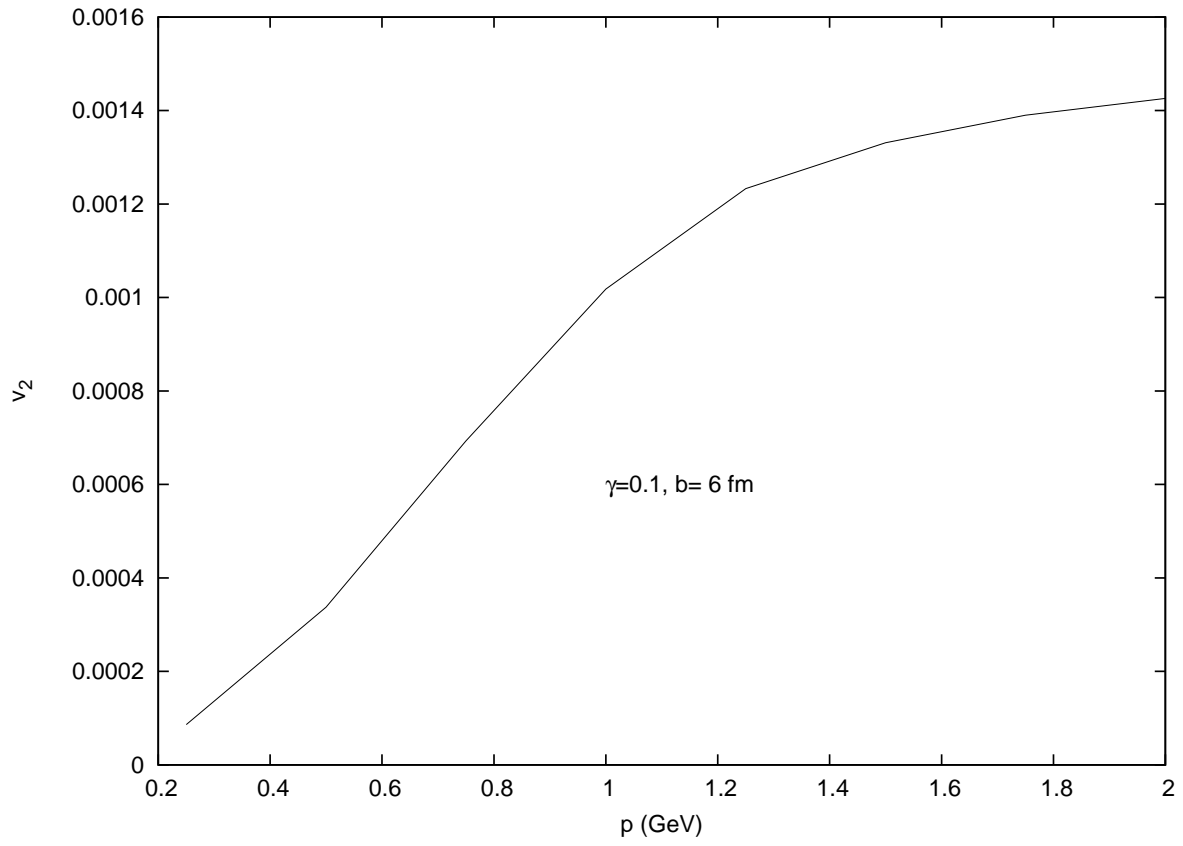


Figure 3: Elliptic flow coefficient  $v_2$  with  $\gamma = 0.1$  as a function of  $p$  at  $b = 6$  fm for Au-Au collisions at  $y = 10$ .

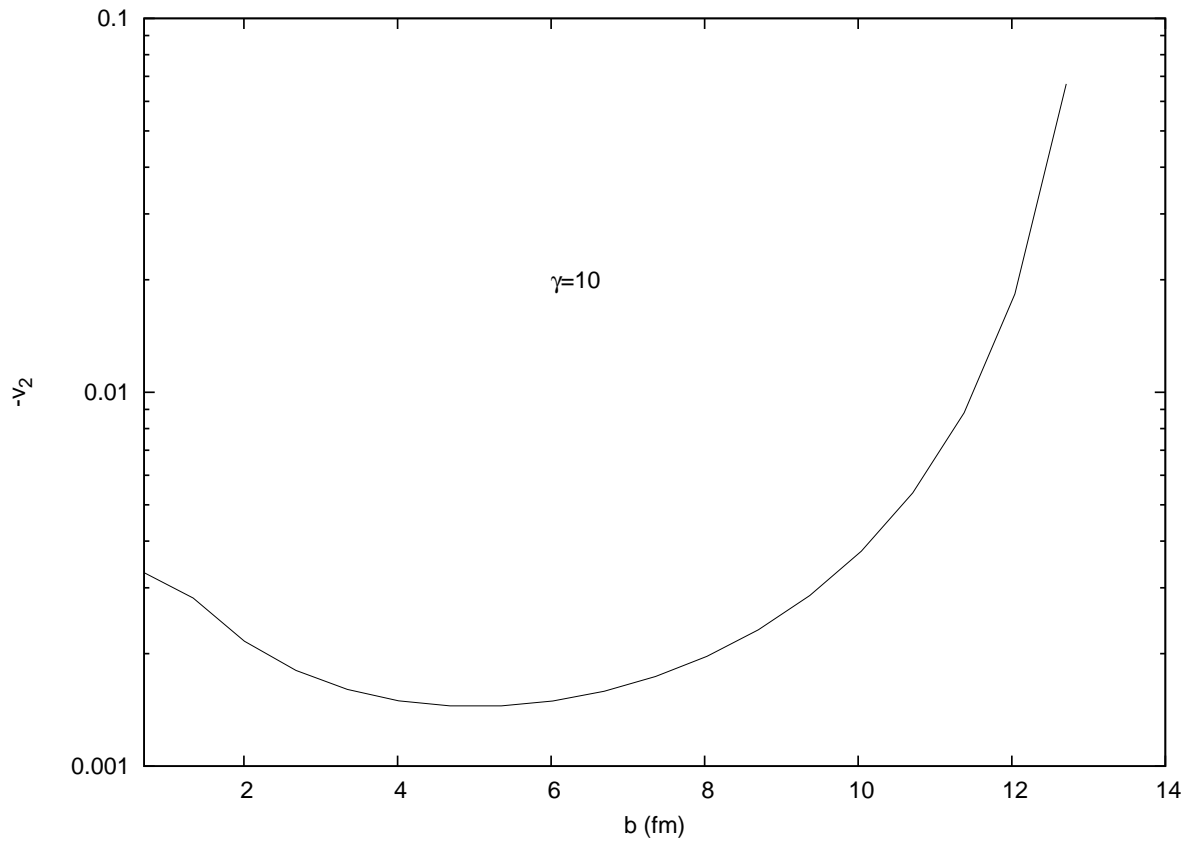


Figure 4: Elliptic flow coefficient  $|v_2|$  with  $\gamma = 10$  as a function of  $b$  for Au-Au collisions at  $y = 10$ .

of string fusion and mentioned in the Introduction. In fact this process is of the same nature as implied in the hydrodynamical approach, a sort of collective interaction. The difference is rather quantitative, since fusion of strings brings the nuclear matter in the overlap to the liquid state gradually, depending on the so-called percolation parameter  $\rho$ , which is the string density in the transverse space. Only at values  $\rho > 1.1 \div 1.2$  drops of nuclear matter (fused strings) on the nuclear scale begin to form and at very high values of  $\rho$  they tend to occupy all the overlap space.

The elliptic flow may have its origin in the fact that fused strings are not symmetric in the transverse plane and therefore may emit particle with different probability in different azimuthal directions. As a source of this asymmetry one may consider quenching of emitted particles as they pass through the fused string area. In this case if a particle is emitted from the forward surface of the fused string it will have a greater momentum than the one emitted from the backward surface, the latter having to pass through the string losing its energy. Generally, if the emitted particle has to propagate inside the string a path of length  $l$  we may assume the probability to see the particle of momentum  $p$  outside the string to be proportional to

$$P(p, l) = e^{-\frac{\xi p^2}{1-\sigma l}}, \quad (32)$$

where  $\sigma$  characterizes the loss of the transverse energy per unit length. If the fused string is not symmetric, then the length  $l$  will depend on the direction of emission, that is on the angle between the  $x$ -axis related to the string and momentum  $\mathbf{p}$ .

By itself this anisotropy of particle emission from fused strings cannot give any elliptic flow. If the overlap is azimuthally symmetric (impact parameter  $b = 0$ ) then obviously strings will occupy arbitrary directions respective to  $\mathbf{b}$  and the resulting distribution in momenta will be fully isotropic. However if the overlap is not symmetric in the azimuthal angle, then fused strings of different directions will form with different probabilities. This will give rise to a non-zero elliptic flow. A clear limiting case is when  $\rho \gg 1$  and all strings fuse into one which occupies all the overlap area and so is unsymmetric if the latter is.

Below we shall try to develop a more quantitative way to calculate the elliptic flow from string fusion. As a typical form of the fused string we shall assume a symmetric almond similar to the shape of the nuclear overlap for collisions of two identical nuclei with radius  $R$  at distance  $b$  between their centers. It is described by the equation

$$\left(x \pm \frac{b}{2}\right)^2 + y^2 = R^2 \quad (33)$$

where  $x$ -axis is directed along its minor axis. The two axes of the almond itself  $a$  and  $d$  with  $a > d$  are

$$a = \sqrt{4R^2 - b^2}, \quad d = 2R - b, \quad b \leq 2R. \quad (34)$$

We shall be interested in the emission of particles at angle  $\chi$  to the minor axis of the almond ( $x$ -axis) in the forward direction. Because of symmetry we can assume  $0 \leq \chi \leq \pi/2$ . Particles emitted at point  $(x_0, y_0)$  in this direction move along the line

$$y = \alpha x + c, \quad c = y_0 - \alpha x_0, \quad \alpha = \tan \chi \quad (35)$$

(see Fig. 5).

Points  $x_1$  and  $x_2$  on the surface of the string from which the particle is emitted in the forward and backward directions respectively are obtained as solutions of the system of equations (35) and

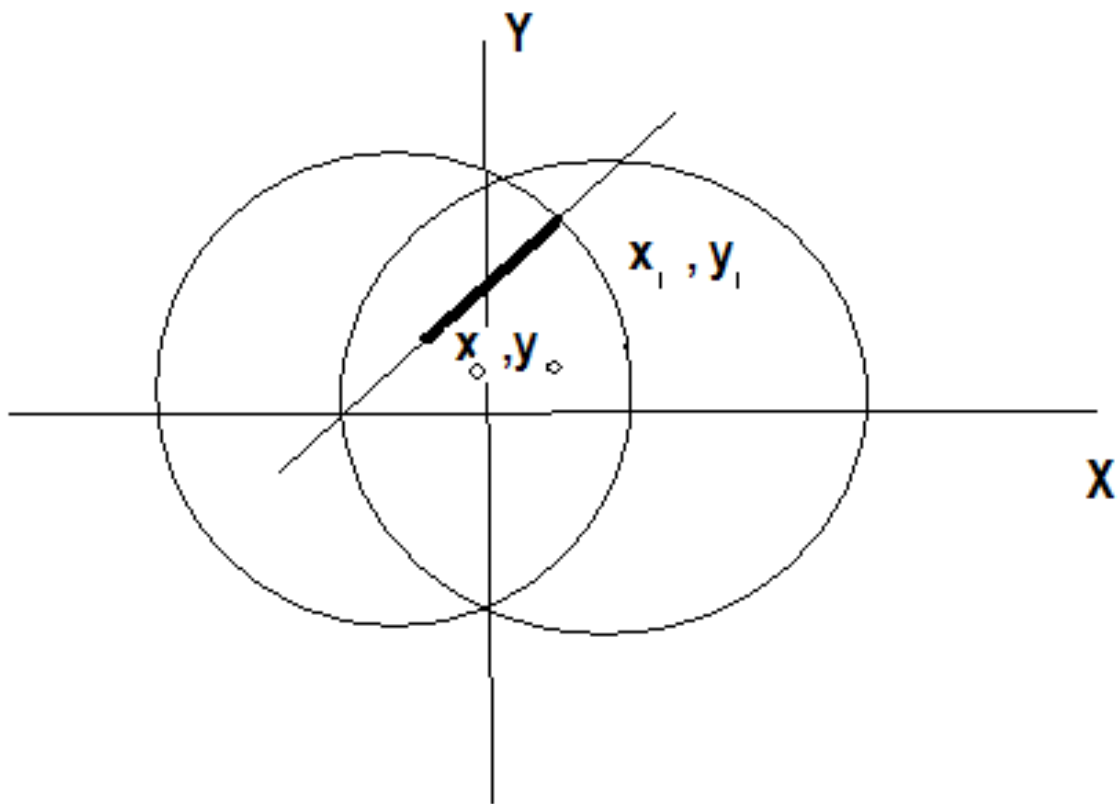


Figure 5: The almond of the nuclear overlap and the path of a particle emitted from point  $(x_0, y_0)$  at a given angle to the minor axis of the diamond

(33) with signs '+' and '-' respectively. They may lie either on different sides of the almond or on the same side depending on the values of  $c$  and  $\alpha$ . Trivial manipulations give

$$x_1 = \frac{1}{\lambda^2} \left( - (+) \frac{b}{2} - \alpha c + \sqrt{Q_{1(2)}} \right), \quad c < (>) \frac{a}{2} \quad (36)$$

and

$$x_2 = \frac{1}{\lambda^2} \left( + (-) \frac{b}{2} - \alpha c - \sqrt{Q_{2(1)}} \right), \quad c > (<) - \frac{a}{2}, \quad (37)$$

where

$$\lambda^2 = 1 + \alpha^2, \quad Q_1 = \lambda^2 R^2 - (c - \alpha b/2)^2, \quad Q_2 = \lambda^2 R^2 - (c + \alpha b/2)^2. \quad (38)$$

The length travelled by the emitted particle in the forward direction is given by

$$l = \sqrt{(x_1 - x_0)^2 + (y_1 - y_0)^2} = \lambda(x_1 - x_0) = \frac{\lambda}{\alpha}(y_1 - y_0). \quad (39)$$

The emission probability will be given by (32). It will depend on the initial emission point  $(x_0, y_0)$  and angle  $\chi$ . To find the total emission probability at given  $p$  and  $\chi$  one has to integrate over all  $(x_0, y_0)$  in the almond area. Up to a constant factor

$$P(p, \chi) = \int dx_0 dy_0 e^{-\frac{\xi p^2}{1 - \sigma l(\chi, x_0, y_0)}}. \quad (40)$$

The total emission probability at given  $\chi$  will be given after integration over all  $p$ . Again up to a constant factor

$$P(\chi) = \int dx_0 dy_0 (1 - \sigma l(\chi, x_0, y_0)). \quad (41)$$

Note that the expression for  $l$  considerably simplifies for the extreme angles  $\chi = 0$  and  $\chi = \pi/2$ . If  $\chi = 0$  then  $\lambda = 1$  and

$$x_1 = -x_2 = \sqrt{R^2 - y_0^2} - \frac{b}{2}. \quad (42)$$

If  $\chi = \pi/2$  then  $\lambda/\alpha = 1$  and

$$y_1 = -y_2 = \sqrt{R^2 - (|x_0| + b/2)^2}. \quad (43)$$

In these cases one can obtain  $P(\chi)$  in an analytical form:

$$P(\chi = 0) = \Omega - \sigma \left[ \frac{2}{3} a(2R^2 + b^2) + bR^2 (2\zeta + \sin(2\zeta)) \right] \quad (44)$$

and

$$P(\chi = \pi/2) = \Omega - \frac{1}{3} \sigma [8R^3 - 6bR^2 + b^3/2], \quad (45)$$

where

$$\zeta = \arccos \frac{b}{2R} \quad (46)$$

and  $\Omega$  is the almond area

$$\Omega = R^2 (2\zeta - \sin(2\zeta)). \quad (47)$$

As mentioned, this anisotropy of emission from an unsymmetric string has to be combined with the anisotropic distribution of strings in the anisotropic overlap. Choose the system in which the  $x$

axis is directed along the impact parameter. Let the minor axis of the almond corresponding to the fused string be directed at azimuthal angle  $\theta$ . Then particle emitted at angle  $\chi$  respective to the minor axis of the almond will be emitted at azimuthal angle  $\phi = \chi + \theta$  respective to the direction of the impact parameter. It is the  $\phi$ -dependence which is measured experimentally, so that in our formulas for the emission probability and length  $l$  one has to put  $\chi \rightarrow \chi - \theta$ . The fused string can be generally directed at any angle  $\theta$  respective to the direction of  $\mathbf{b}$  with the probability  $D(\theta)$ . So the final distribution in the transverse momentum of particles emitted from this fused string will be obtained as

$$\frac{d\sigma}{pdpd\phi} = C \int d\theta D(\theta) P(p, \phi - \theta) \quad (48)$$

and the distribution in  $\phi$  as:

$$\frac{d\sigma}{d\phi} = C_1 \int d\theta D(\theta) P(\phi - \theta). \quad (49)$$

Obviously if the distribution of strings in  $\theta$  is isotropic, then integration over  $\theta$  will eliminate any dependence on  $\phi$ .

If the overlap is fully symmetric ( $b = 0$ ) then obviously we cannot expect any dependence of the string distribution in  $\theta$ . However if it is not then such a dependence certainly arises.

To see this, take the percolation parameter  $\rho$  to be very large, so that practically all strings in the overlap area fuse into a single cluster, which occupies the whole overlap volume. With an asymmetric overlap the only possibility to form such a cluster is to direct its major and minor axes along the major and minor axes of the overlap. In other words the distribution of strings in  $\theta$  acquires a  $\delta$ -function form

$$D(\theta) = \delta(\theta) \quad (50)$$

and then

$$\frac{d\sigma}{pdpd\phi} = CP(p, \phi), \quad (51)$$

$$\frac{d\sigma}{d\phi} = C_1 P(\phi) \quad (52)$$

where the almond occupies the whole overlap area, so in  $P$  one has to put  $R = R_A$ , the radius of colliding nuclei, and  $b$  the actual impact parameter. The obtained asymmetry is quite similar to the one in the well-known mechanisms in which the emitted particles are suppressed by final-state interactions as they pass through the overlap area [11].

The string fusion mechanism allows to obtain something more: the dependence of the suppression on the string density through the percolation parameter taking not so high values. Then strings occupy only part of the overlap area given by factor

$$F(\rho) = 1 - e^{-\rho}. \quad (53)$$

This gives them a possibility to form different clusters and have different directions in the overlap area. If  $\rho$  and so the string length  $l$  become small all directions become equally possible, so that the distribution in  $\theta$  becomes flat and with that the distribution in  $\phi$ .

Unfortunately to study this  $\rho$ -dependence accurately one has to recur to a very complicated numerical Monte-Carlo methods to be able to see forms and directions of the string clusters in detail.

To avoid this we may use a crude simplified approach. We may assume that strings (fused and simple) on the average are distributed homogeneously in the overlap area. Again on the

average, an emitted particle has to pass through the string matter length  $l$  which is smaller than the corresponding length at  $\rho \gg 1$  by factor

$$\kappa_1(\rho) = \sqrt{F(\rho)}. \quad (54)$$

The average string tension will be greater than for the single string by factor  $\kappa(\rho)^{-1}$  where

$$\kappa(\rho) = \sqrt{\frac{1 - e^{-\rho}}{\rho}} = \frac{\kappa_1}{\sqrt{\rho}}. \quad (55)$$

The distribution in the transverse momentum will then be given by the same formulas (51) and (52) with the appropriate rescaling of  $l$  and  $\xi$

$$\frac{d\sigma}{pdpd\phi} = CP(p, \phi, \xi \rightarrow \xi\kappa, l \rightarrow \kappa_1 l) = C \int dx_0 dy_0 e^{-\frac{\kappa(\rho)\xi p^2}{1 - \sigma\kappa_1(\rho)l(\phi, x_0, y_0)}} \quad (56)$$

$$\frac{d\sigma}{d\phi} = C_1 P(\phi, a \rightarrow a\kappa, l \rightarrow \kappa_1 l) = \frac{C_1}{\kappa(\rho)} \int dx_0 dy_0 (1 - \kappa_1(\rho)\sigma l(\phi, x_0, y_0)) \quad (57)$$

This approach will be referred to as the 'averaged model'.

Note that distribution (56) formally may be interpreted as following from the dependence of the percolation parameter  $\rho$  on the point inside the overlap. Indeed one can rewrite (56) in the form

$$\frac{d\sigma}{pdpd\phi} = C \int dx_0 dy_0 e^{-\kappa\rho_{eff}(\phi, x_0, y_0)\xi p^2}, \quad (58)$$

where the point- and direction-dependent effective percolation parameter is determined by the obvious relation

$$\sqrt{\frac{\rho_{eff}(\phi, x_0, y_0)}{1 - e^{-\rho_{eff}(\phi, x_0, y_0)}}} = \frac{\sqrt{\rho}}{\sqrt{1 - e^{-\rho}}} - \sigma\sqrt{\rho}l(\phi, x_0, y_0). \quad (59)$$

In this way this picture coincides with the one proposed in [17] and may be considered as its justification.

Calculations become especially simple if we neglect higher harmonics in the expansion in  $\cos(n\phi)$  and restrict to  $n = 2$ . Then we can obtain the elliptic flow coefficient by comparing emission at angles  $\phi = 0$  and  $\phi = \pi/2$ . In this case for the distribution integrated over  $p$  we get an explicit expression

$$\begin{aligned} 2v_2 &= \frac{P(0) - P(\pi/2)}{P(0) + P(\pi/2)} \\ &= \frac{1}{2} \frac{\epsilon(\rho) \left[ 8 - 6b + b^3/2 - 2a(2 + b^2) - 3b(2\zeta + \sin(2\zeta)) \right]}{2 - \epsilon(\rho) \left[ 8 - 6b + b^3/2 + 2a(2 + b^2) + 3b(2\zeta + \sin(2\zeta)) \right]}, \end{aligned} \quad (60)$$

where

$$\epsilon(\rho) = \frac{\kappa_1 \sigma R_A}{3\Omega} \quad (61)$$

and we have put  $R_A \rightarrow 1$  everywhere else, so that

$$\Omega = 2\zeta - \sin(2\zeta), \quad \zeta = \arccos \frac{b}{2} \quad (62)$$

and  $a$  and  $b$  are to be measured in units  $R_A$ .

A more elaborate picture ('elaborate model'), leading to a non-trivial  $\theta$ -dependence of  $D(\theta)$ , can be based on the assumption that the macroscopic string cluster has the same almond shape as the overlap itself but its dimension is reduced by factor  $\kappa$ . Then its direction may vary and the distribution of strings in  $\theta$  will not be so sharply peaked at  $\theta = 0$ . Accordingly we assume the length of the major axis of the string is

$$a = \kappa_1 \sqrt{4R_A^2 - b^2} \equiv \kappa_1 a_0 \quad (63)$$

Its direction respective to the direction of  $\mathbf{b}$  will be given by  $\tau = \theta + \pi/2$ . Symmetry of the almond dictates that the distribution does not change if  $\theta \rightarrow -\theta$  and  $\theta \rightarrow \pi - \theta$ . So it is sufficient to consider the case when the major axis of the string has its angle  $\tau$  contained in the interval between 0 and  $\pi/2$  which corresponds to  $-\pi/2 < \theta < 0$ . Values of  $D(\theta)$  at other angles will be obtained by symmetry.

The probability that the string of dimension  $l$  and major axis forming angle  $\tau$  with the direction of  $\mathbf{b}$  is proportional to the part of almond area  $A$  in which such a string can lie. This area is given by the integral over the almond area over points  $\mathbf{x}$  and  $\mathbf{x}'$  such that they lie on a line forming angle  $\tau$  with the  $x$ -axis and with  $|\mathbf{x} - \mathbf{x}'| = l$ . From (39) we find

$$A = \int \int d^2\mathbf{x} d^2\mathbf{x}' \delta(x' - x - l/\lambda) \delta(y' - y - \alpha l/\lambda) \quad (64)$$

where  $\alpha = \tan \tau$  and  $\lambda = \sqrt{1 + \alpha^2}$ . The average length  $l$  of the string will be given by Eq. (63). The two-dimensional integral (64) can be easily calculated numerically. Note, that as follows from these numerical calculations, with the growth of  $b$  and  $\rho$ , the distribution proportional to  $A$  rapidly takes the form of the  $\delta$ -function, concentrated at  $\tau = \pi/2$ , that is at  $\theta = 0$ , which returns us to the previously considered averaged approximation. So using this more elaborate picture is only reasonable at relatively small values of  $b$  and  $\rho$ .

## 5.2 Numerical results

Our model contains a single new parameter  $\sigma$  which characterizes the loss of energy in passing through the string field. In fact by dimensional reasons  $\sigma$  is proportional to the nuclear radius  $R_A$ . Taking  $R_A = R_0 A^{1/3}$  we find

$$\sigma = \sigma_0 A^{1/3} \quad (65)$$

where  $\sigma_0$  is a dimensionless and  $A$  independent parameter to be extracted from the experimental data.

Values of the percolation parameter  $\rho$  corresponding to given values of the impact parameter  $b$  were taken from [12] for Au-Au collisions at 62.4 and 200 GeV. They are shown in Fig. 6.

Calculations of the elliptic flow coefficient  $v_2$  from events integrated over the transverse parameter as a function of impact parameter  $b$  according to the averaged formula (57) give the results shown in Fig 7 for Au-Au collisions at 62.4 and 200 GeV. Calculations according to the same averaged picture (Eq. (56) of the transverse momentum dependence are presented in Fig 8 for central, mid-central and peripheral collisions. In both cases quenching parameter  $\sigma_0$  was adjusted to the mid-central results for events integrated over transverse momenta. The adjusted value was  $\sigma_0 = 0.09$ .

Passing to our elaborate model, with a non-trivial distribution in  $\theta$ , we, as mentioned, have found that with the growth of  $\rho$  this distribution rapidly takes the form of a  $\delta$  function. This is



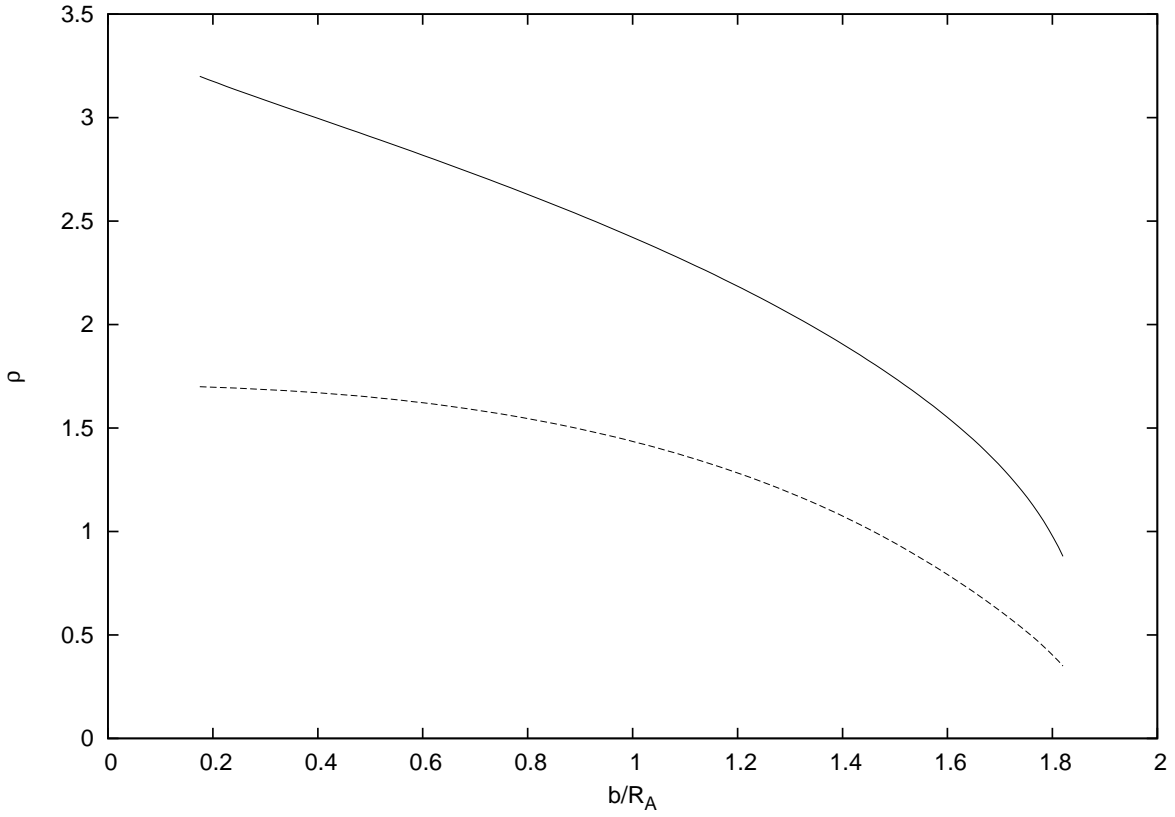


Figure 6: Percolation parameter as a function of impact parameter for Au-Au collisions at 62.4 (lower curve) and 200 GeV borrowed from [12]

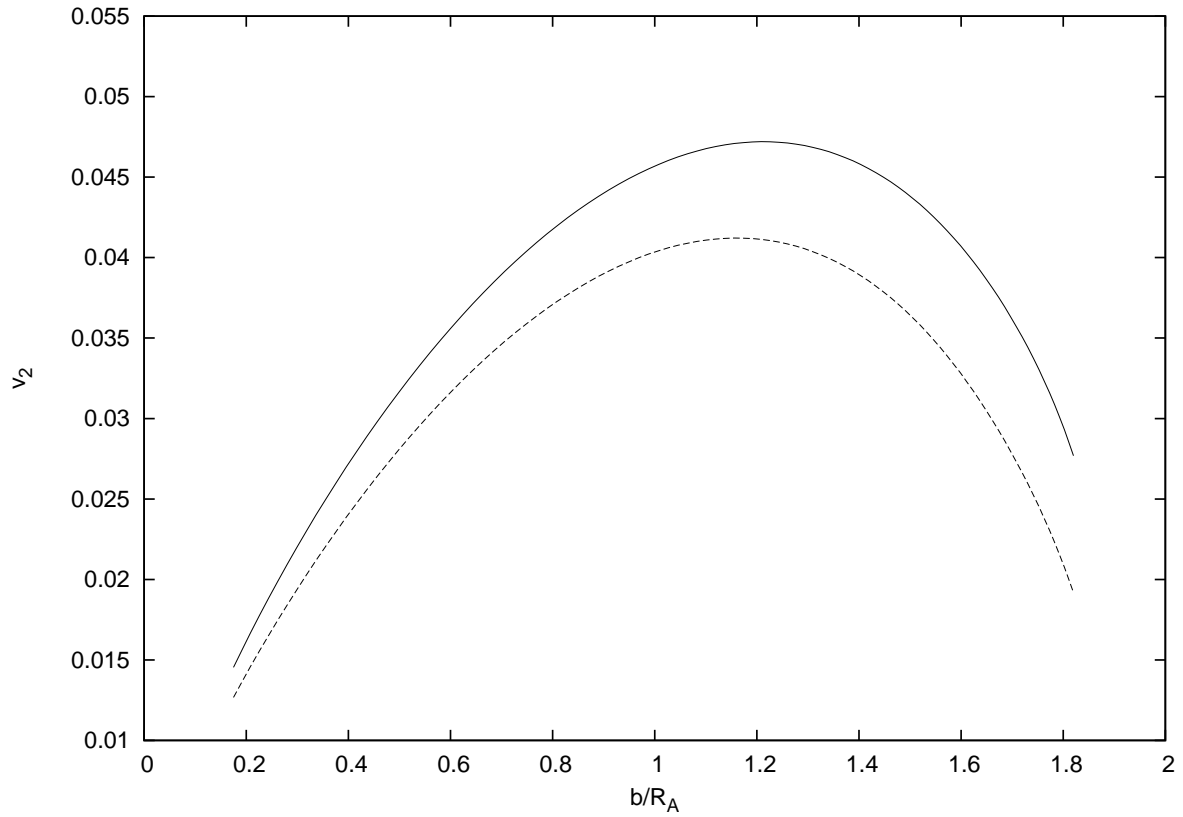


Figure 7:  $v_2$  as a function of impact parameter for Au-Au collisions at 62.4 (lower curve) and 200 GeV according to Eq. (57)

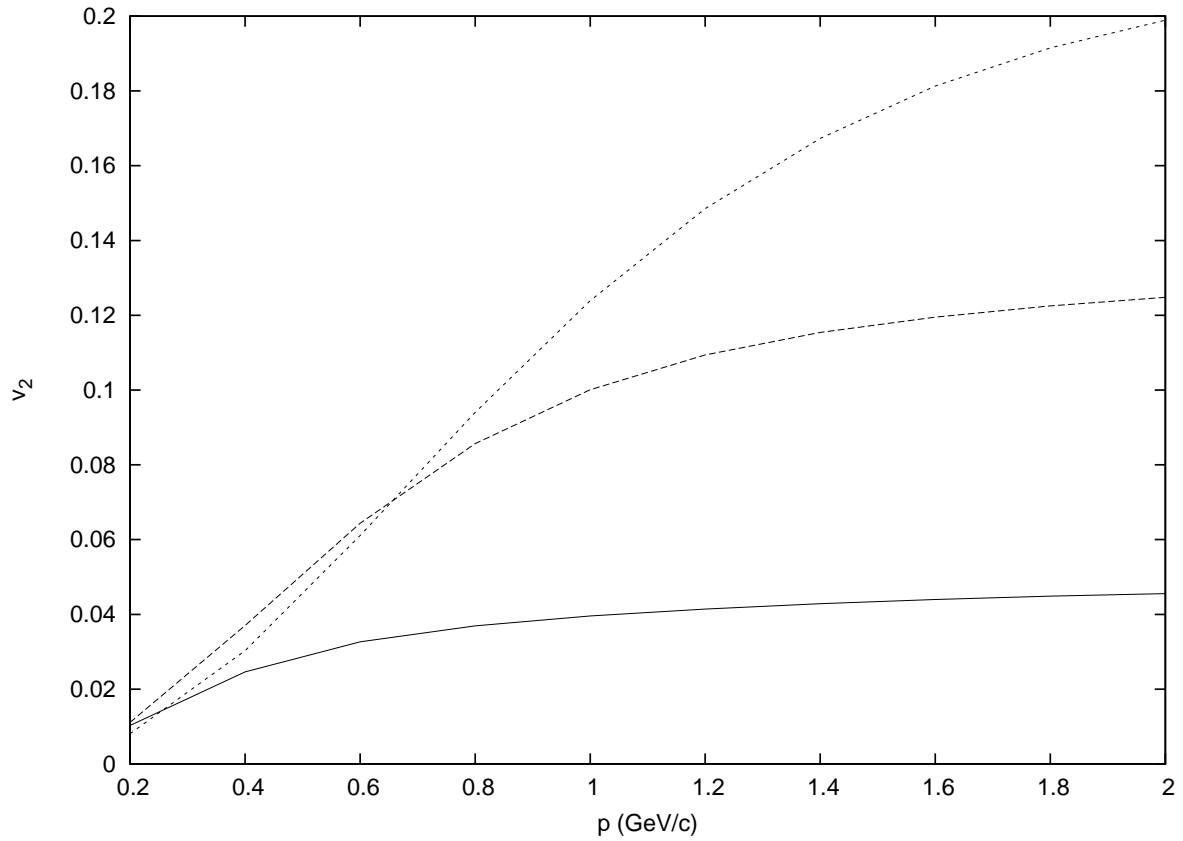


Figure 8:  $v_2$  as a function of transverse momentum for Au-Au collisions at 200 GeV according to Eq. (56) for peripheral (uppermost curve), mid-central and central (lowest curve) collisions

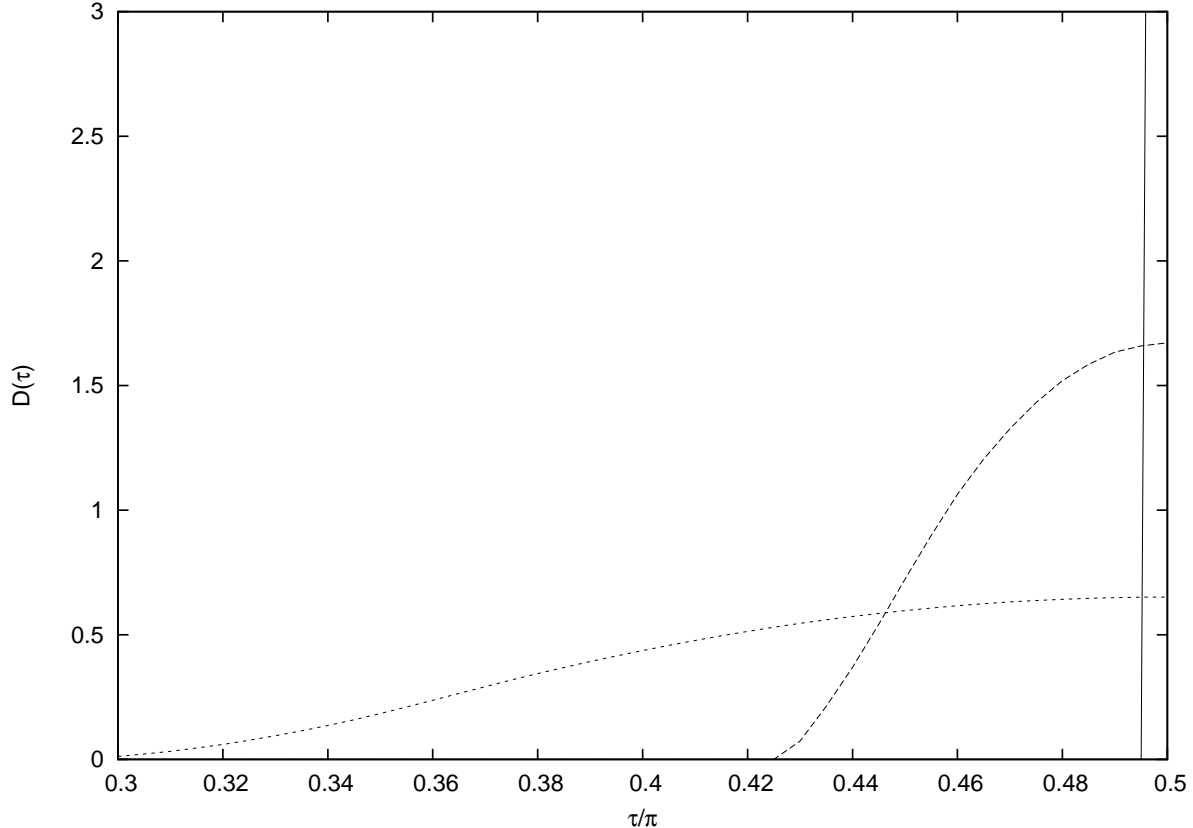


Figure 9: The distribution  $D(\theta)$  as a function of  $\tau = \pi/2 - \theta$  for  $b = R_A$  and  $\rho = 0.5$  (the leftmost curve), 1.0 (the middle curve) and  $\rho = 2$ . (the rightmost curve, of which only the lowest part is shown)

illustrated in Fig. 9 where we plot this distribution as a function of angle  $\tau = \pi/2 - \theta$  for  $b = R_A$  and  $\rho = 0.5, 1$  and  $2$ . As one can see for  $\rho = 2$  the distribution is completely concentrated at  $\theta = 0$

Turning to the data for  $b$  and  $\rho$  in Fig 6 we find that for all their values for Au-Au collisions at 200 GeV the distribution  $D(\theta)$  is practically given by  $\delta(\theta)$  so that our more elaborate model gives nothing new as compared the previous crude one. Calculations for Au-Au collisions at 62.4 GeV, for which the distribution  $D(\theta)$  is well different from a  $\delta$ -function give however results which are also practically identical with the averaged model. This is illustrated in Fig. 10 in which we compare  $v_2$  for events integrated over transverse momenta as a function of  $b$  for Au-Au collisions at 62.4 GeV calculated according to Eqs. (49) and (64) Eq. (57) with  $\sigma_0 = 0.09$ . The difference is negligible. So the sophistication implied in the our elaborate model turns out to have no practical value.

On the purely theoretical level one expects that the elaborate model places more emphasis on string fusion, so that it should give much less  $\phi$  dependence at low values of  $\rho$  below the percolation threshold  $\rho \sim 1.1 \div 1.2$ . This is indeed so as shows Fig. 11 in which we plot  $v_2$  for averaged and elaborate models at fixed  $b = R_A$  as a function of  $\rho$  at comparatively low values. One observes that at values of  $\rho$  below the percolation the non-trivial model gives  $v_2$  substantially smaller than the averaged one.

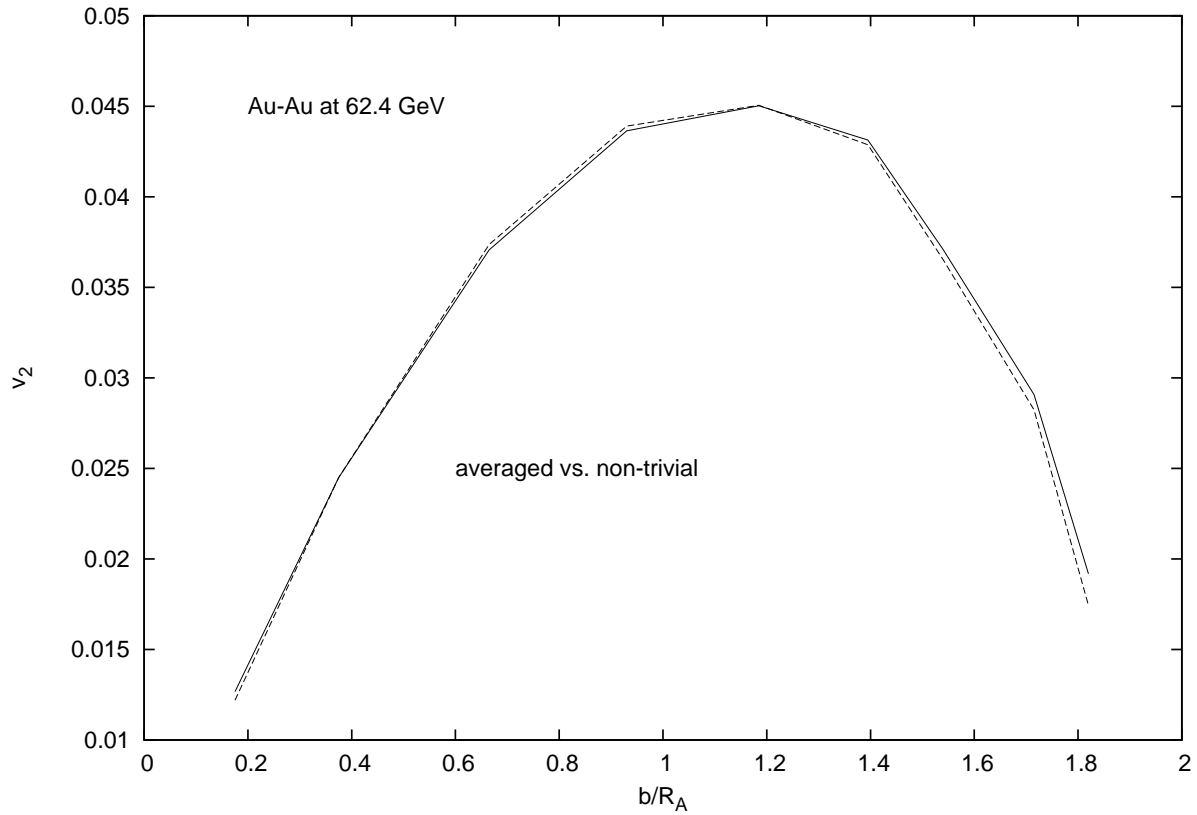


Figure 10:  $v_2$  calculated in the averaged (solid curve ) and elaborate models for Au-Au collisions at 62.4 GeV as a function of  $b$  with  $\sigma_0 = 0.09$

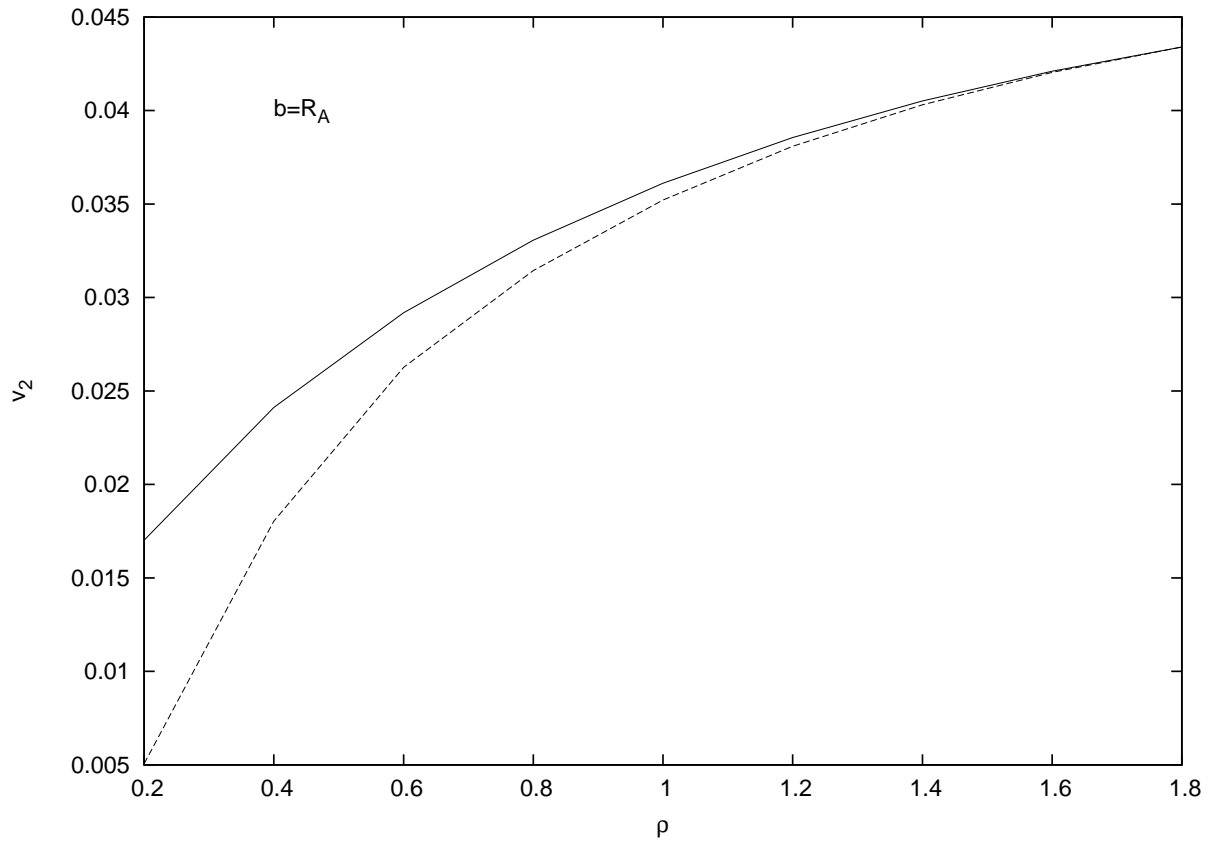


Figure 11:  $v_2$  calculated in the averaged (solid curve) and elaborate models for Au-Au collisions at fixed  $b = R_A$  quenching parameter  $\sigma_0 = 0.09$  and  $\rho$  changing from 0.2 to 1.8.

## 6 Conclusions

We have demonstrated that the colour string model with fusion and percolation can successfully describe the observed elliptic flow in high-energy heavy ion collisions. An important ingredient in this description is anisotropy of the string emission spectra in the azimuthal direction. This may follow both from the string propagation in the transverse plane due to a non-zero pomeron slope and from quenching of the emitted partons in the strong colour field inside the string. We have found that the first source of anisotropy plays a minor role at accessible energies due to the fact that the distance travelled by the string in the transverse plane turns out to be small. The second source of anisotropy however gives rise to anisotropy, which, upon adjusting the parameter of quenching, allows to describe the data quite well both in their centrality dependence and their transverse momentum dependence.

Our results have been obtained under some substantial approximations. In the simplest case we used the over-all averaged picture both as to the form of the string clusters as to their distribution in the nuclei overlap. In the more elaborate case we fixed the geometric form of the leading cluster and then found its distribution in the overlap. Both approximations have led to practically the same results. Still careful comparison demonstrates that the leading cluster approximation gives less flow at small values of the percolation parameter, which indicates that string percolation is the most important source of the flow. The results obtained here are similar to previous calculations in [17, 18] in the same framework of percolation of strings under different approximations.

More accurate calculations of the flow in the string percolation model are only possible in the developed Monte-Carlo approach. They do not seem simple since one has to find an overall quenching for a given distribution of string clusters in the overlap. We plan to conduct such calculations in future.

## 7 Acknowledgements

This work is done under the projects FPA2008-01177 and Consolider of the Ministry of Science and Innovation of Spain and under the project of Xunta de Galicia. One of the authors (M.A.B) is indebted to the University of Santiago de Compostela for attention and financial support. He has also benefited from grants RFFI 09-012-01327-a and RFFI-CERN 08-02-91004 of Russia which partially supported this work.

## References

- [1] N.Borghini and U.A.Wiedemann, *J.Phys.*, **G 35** (2008) 023001.
- [2] J.Y.Ollitrault, *Phys. Rev.*, **D 46** (1992) 229.
- [3] K.G.Boreskov, A.B.Kaidalov, O.V.Kancheli, *Eur. Phys. J C* **58** (2008) 445..
- [4] N.Armento, M.A.Braun, E.G.Ferreiro and C.Pajares, *Phys. Rev. Lett.* **77** (1996) 3736; M.Nardi and H.Satz. *Phys. Lett.* **B 442** ((1998) 14.
- [5] M.A.Braun and C.Pajares, *Phys. Rev. Lett.*, **85** (2000) 4864.
- [6] M.A.Braun and C.Pajares, *Eur. Phys. J.*, **C 16** (2000) 349.

- [7] M.A.Braun, C.Pajares and J.Ranft, Int. J. Mod. Phys., **A 14** (1999) 2689.
- [8] M.A.Braun, F.del Moral and C.Pajares, Phys. Rev., **C 65** (2002) 024907.
- [9] J.Dias de Deus, E.G.Ferreiro, C.Pajares and R.Ugoccioni, Eur. Phys. J., **C 40** (2005) 229
- [10] L.Cunqueiro, J.Dias de Deus, E.G.Ferreiro and C.Pajares, Eur. Phys. J., **C 53** (2008) 585
- [11] A.Capella and E.G.Ferreiro, Phys. Rev. **C 75** (2007) 024905.
- [12] T.J.Tarnowsky, B.Srivastava, R.Scharenberg (STAR collab), Nukleonika51S3 (2006) S109-S112 (arXiv: nucl-ex/0606019).
- [13] S.S.Adler *et al*, PHENIX collab., Phys. Rev. Lett., **91** (2003) 182301; Phys. Rev. **C 77** (2008) 014906
- [14] A.Adare *et al*, PHENIX collab., Phys. Rev. Lett., **98** (2007) 242302.
- [15] B.Alver *et al*, PHOBOS collab., Phys. Rev. Lett., **98** (2007) 162301.
- [16] S.A.Voloshin ( STAR collab.), J.Phys., **G 34** (2007) 5883.
- [17] I.Bautista, L.Cunqueiro, J.Dias de Deus and C.Pajares, J.Phys., **G 37** (2010) 015103.
- [18] I.Bautista, J.Dias de Deus and C.Pajares, arXiv:1007.5206 [hep-ph].